Research Article | Vol. 28, No. 26 / 21 December 2020 / Optics Express 39640
Optics EXPRESS

Hydrogel based Fabry-Pérot cavity for a pH sensor

ABDULLAH AL NOMAN,[1] JITENDRA NARAYAN DASH,[2] XIN CHENG,[2,3] CHERN YANG LEONG,[2] HWA-YAW TAM,[2] AND CHANGYUAN YU[1,4]

[1]*Photonics Research Center, Department of Electronic and Information Engineering, The Hong Kong Polytechnic University, 11 Yuk Choi Rd, Hung Hom, Hong Kong SAR, China*
[2]*Photonics Research Center, Department of Electrical Engineering, The Hong Kong Polytechnic University, 11 Yuk Choi Rd, Hung Hom, Hong Kong SAR, China*
[3]*eechengx@polyu.edu.hk*
[4]*changyuan.yu@polyu.edu.hk*

Abstract: A simple, reliable, and quick reactive Fabry-Pérot (FP) structure-based fiber optic pH sensor is presented. The pH-sensitive hydrogel and single-mode fiber (SMF) are placed inside a fused silica capillary to form the FP cavity. The gel thickness is characterized by the spin coating method with respect to different spin speeds. The proposed sensor shows a pH sensitivity of 0.30 nm/pH along with a fast response time of 15 s to 20 s for different pH solvents in the acidic range. Also, the temperature sensitivity of the FPI sensor is found to be -0.56 nm/°C.

1. Introduction

pH detection is one of the most vital features in several fields of sciences, such as environmental, biomedical, chemical, and agricultural [1]. The concept of cheap, reliable, and compact pH sensor monitoring is continuously progressing since the 1980s. Many chemical manufacturing production requires precise, real-time pH level detection. Furthermore, there is a specific necessity to measure pH on minor scales in the biochemical and biomedical region [2]. Mostly, acid and base pH level solutions are determined by the glass electrodes or strips of paper. Both sensors have benefits and drawbacks; for instance, paper strips indicate only the pH color level instead of exact numerical values; in contrast, glass electrodes provide precise values. However, they are costly and do not have a real-time monitoring system [3]. These existing disadvantages motivate to improvise pH devices. Thus, optical fiber-based pH sensors get the attention due to the compact size, low-cost, highly sensitive, and no electromagnetic interference features, where the optical signal made fiber commendable in all medium.

To date, various fiber optic-based pH sensors have been investigated based on either intensity interrogation or wavelength interrogation. A dye molecules coated fiber has been utilized for pH sensing based on intensity interrogation [4]. Another intensity based pH sensor has been demonstrated using fluorescence material coated polymer optical fiber (POF) [5]. However, intensity based pH sensors are vulnerable to fluctuation in source power and other external factors. In contrast, wavelength based sensors are more reliable due to their stability and high accuracy. For instance, hydrogel (poly (ethylene glycol) diacrylate (PEGDA)) coated fiber Bragg grating (FBG) has been proposed for pH sensing where the wavelength shift occurred due to the compression of hydrogel [6]. Furthermore, a bio-compatible pH sensor based on 1,4 butanediol diacrylate (BDDA) and piperazine (PIP) mixer has been demonstrated using thin core interferometric technique [7]. Besides, pH sensors based on the surface plasmon resonance (SPR) method have also been reported [8]. However, fabrication of the aforesaid sensors involves complicated steps and they are bulky and less sensitive to pH variation.

#414636 https://doi.org/10.1364/OE.414636
Journal © 2020 Received 10 Nov 2020; revised 7 Dec 2020; accepted 7 Dec 2020; published 15 Dec 2020

Optics EXPRESS

Meanwhile, fiber-optic Fabry-Pérot interferometers (FPI) have been utilized for various sensing applications due to their distinct features such as compact size, reliable, and simple fabrication process [9–13]. For example, an optical fiber-based pH sensor coated with hydrogel (polyacrylic acid (PAA) and polyvinyl alcohol (PVA) mixed) has been reported for the pH range of 4.1-6.9 [14]. J. Goicoechea *et al.* have reported an FPI based pH sensor coated with PAA and polyallylamine hydrochloride (PAH), and the probe has been found to have sensitivity of 0.051 nm/pH along with response time of 3 minutes [15]. However, all above sensors have lesser sensitivity [15], longer response time [14,15] and their detection is confined to smaller pH range [6,14,15].

Here, we reported simple and dependable hydrogel coated FP based fiber optic pH sensor. Due to their specific properties, such as non-hazardousness and biocompatibility, hydrogels have found numerous applications in the biomedical area [16] along with ionic strength [17], and alterations in pH [18,19]. The fabrication of the probe involves coating of a section of fused silica capillary (drawn by our group) with hydrogel followed by insertion of FBG incorporated SMF into the fused silica capillary. The FBG has been included to monitor the environmental temperature. The hydrogel has been coated using the spin coating technique where parameter such as rotation speed has been optimized.

2. Sensor operating principle and fabrication

2.1. Sensing principle

The schematic of the FPI based sensor is shown in Fig. 1. Light reflected from the tip of SMF and the hydrogel interfere with each other to produce the resulting interference pattern. The reflection coefficients of the two surfaces can be determined by the Fresnel reflection equation for normal incidence of light and can be expressed as

$$R_1 = \left|\left|\frac{n_f - n_a}{n_f + n_a}\right|\right|^2; \quad R_2 = \left|\left|\frac{n_a - n_m}{n_a + n_m}\right|\right|^2 \tag{1}$$

where R_1, and R_2 refer to the reflection coefficient of the two surfaces and n_a, n_f, and n_m (1.452) refer to refractive index (RI) of air, core of SMF, and hydrogel, respectively. The preferred hydrogel has higher RI compared to water (1.33), because it only contains 5% to 30% of water by weight.

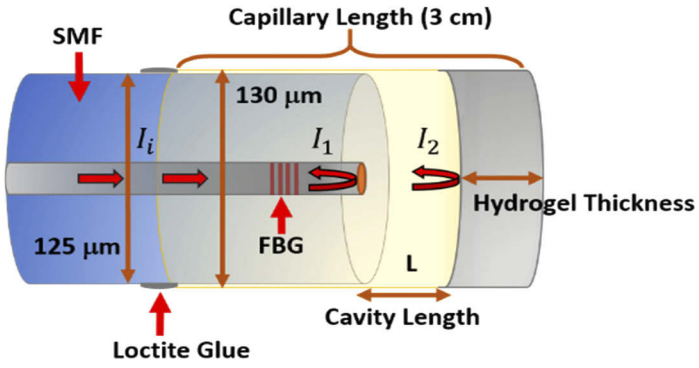

Fig. 1. Schematic diagram of the proposed FPI based sensor.

Due to the low reflectivity from both silica-air (3.5%) and hydrogel-air (3.4%) interfaces, the higher-order reflections may be neglected [20]. The intensity (I_t) of the resultant interference

Optics EXPRESS

pattern can be written as [21–24]

$$I_t = I_1 + I_2 + 2\sqrt{I_1 I_2}cos\left(\frac{4\pi n_a L}{\lambda} + \varphi_i\right)$$
$$I_t = I_i \left\{ \begin{array}{l} R_1 + (1-R_1)(1-\alpha)R_2 + \\ 2\sqrt{(1-R_1)(1-\alpha)R_1 R_2}\ cos\left(\frac{4\pi n_a L}{\lambda} + \varphi_i\right) \end{array} \right\} \quad (2)$$

where I_1 and I_2 refer to the intensity of light reflected from the SMF tip and hydrogel inner surface, respectively. On the other hand, I_i, λ, L, α and φ_i refers to the input light intensity, wavelength of the incident light, cavity length (air gap between the fiber end and hydrogel), transmission loss of the cavity, and the primary phase of the interference, respectively. The free spectral range (FSR) of the interference pattern can be expressed by Eq. (3) [12], where λ_1 and λ_2 refer to the wavelength of the consecutive minima of the interference pattern.

$$\Delta\lambda = \lambda_2 - \lambda_1 = \frac{\lambda_1 \lambda_2}{2n_a L} \quad (3)$$

The sensing principle of the interferometer is based on the shift of the interference minima that occurs due to the change in cavity length. The change in cavity length depends upon the swelling of the hydrogel, which in turn depends upon hydrogen ions (H^+) presents in a solution with specific pH. The chemical equation corresponding to the expansion of the hydrogel can be seen from Eq. (4).

$$[RCOO^-]_{gel} + [H^+]_{aq} = [RCOOH]_{gel} \quad (4)$$

2.2. Fabrication of the proposed sensor:

The schematic of the proposed interferometer is illustrated in Fig. 1. In order to fabricate the sensor, the tip of a section of the capillary (outer diameter: 200 µm, inner diameter: 130 µm, see Fig. 2(a)) is dipped into the hydrogel. The coated tip of the capillary was fixed onto the rotational stage of the spin coating machine, and the rotational speed of the stage was set at 4000 rpm. This process resulted in the formation of a hydrogel coated capillary tip with a smooth inner surface. Thereafter, the tip of the probe is placed under a UV source (CSD-B61-86F, COUSZ, Wuxi, China) so that the hydrogel at the tip of the capillary gets cured. Then a section of flat cleaved FBG inscribed SMF was inserted into the capillary using the translational stage (Nanomax 350/M, Thorlabs, USA, see Fig. 2(b)) and the other end of the SMF was connected to one of the port of a circulator while the other ports of the circulator were connected to a broadband source (BBS) and an optical spectrum analyzer (OSA). This process helps to observe the real time interference reflection spectra produced by the FP cavity during the insertion of SMF into the capillary. Upon achieving the desired interference pattern with good contrast, the SMF was fixed with the inner wall of the capillary using adhesive glue (LOCTITE 431, Henkel, Düsseldorf, Germany). It is to be noted here that the FBG inscribed SMF helps in monitoring the temperature of the ambient environment, thereby leading to the measurement of cross temperature error with better accuracy. The fabricated sensor probe was shown in Fig. 2(c).

Optics EXPRESS

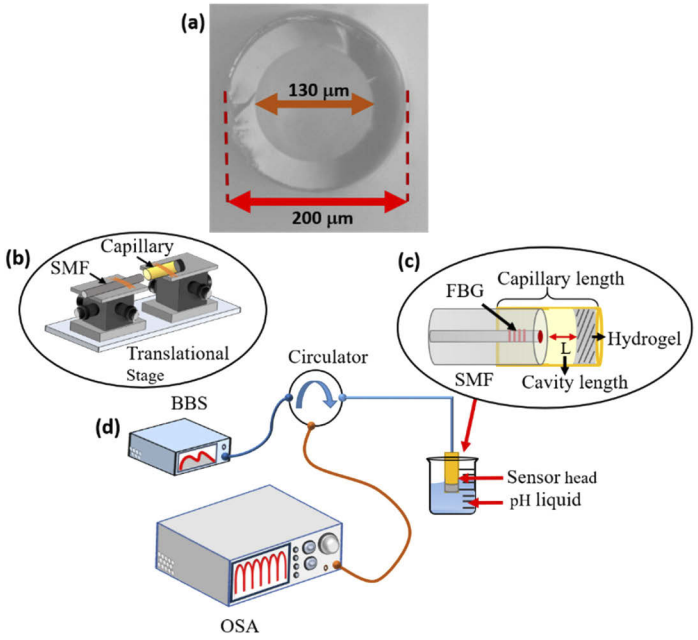

Fig. 2. (a) Capillary cross-section view, (b) the alignment setup, (c) schematic of the fabricated probe, (d) experimental setup.

3. Materials, hydrogel characterization, and experimental setup

3.1. Materials

All chemical materials without any purification were purchased from Sigma Aldrich to fabricate the hydrogel. The following chemicals were used to synthesize the hydrogel: methacrylic acid, MAA (99%, 250 ppm inhibitor), 2-hydroxyethyl methacrylate, HEMA (≥99%, contains ≤50 ppm inhibitor), ethylene glycol dimethacrylate, EGDMA (98%, includes 90-110 ppm inhibitor), and 2, 2-dimethoxy-2-phenylacetonphenone, DMPA (99%). The gel was prepared by mixing of 3.7995 g HEMA (76 wt%), 1.0009 g MAA (20 wt%), 0.1577 g EGDMA (3 wt%), and 0.0527 g (1 wt%) [25], whereas DMPA directly dissolved in the mixture solution of MAA, HEMA and EDGMA.

3.2. Characterization of hydrogel

The thickness of the hydrogel inside the capillary has been characterized by the spin coating method. In this process, the fabricated hydrogel was pre-cured for 15 s by a UV light source so that the liquid viscosity got increased slightly. This made it easier to place the hydrogel inside the silica capillary due to the surface tension [26]. The capillary was then immersed into the gel for 2 s, and the same coated capillary was used for spin coating. This procedure formed a smooth inner layer of hydrogel at the capillary tip, and the gel-coated capillary was again cured for roughly 10 minutes to make it solid. The thickness of the gel and inner surface could be controlled by rotation speed. Figure 3 illustrates the variation in gel various thickness respect to varying spin speed for the fixed time duration. All the measurements have been repeated for three cycles, and the average of the results along with error bars are exhibited in the same figure. The probe having gel thickness of 642.03 µm (corresponding to the rotation speed of 4000 rpm) has been considered for the experiment. The probes with other thickness value have been ruled out due to several reasons, e.g., lower fringe contrast, instability, and rough internal surface.

Optics EXPRESS

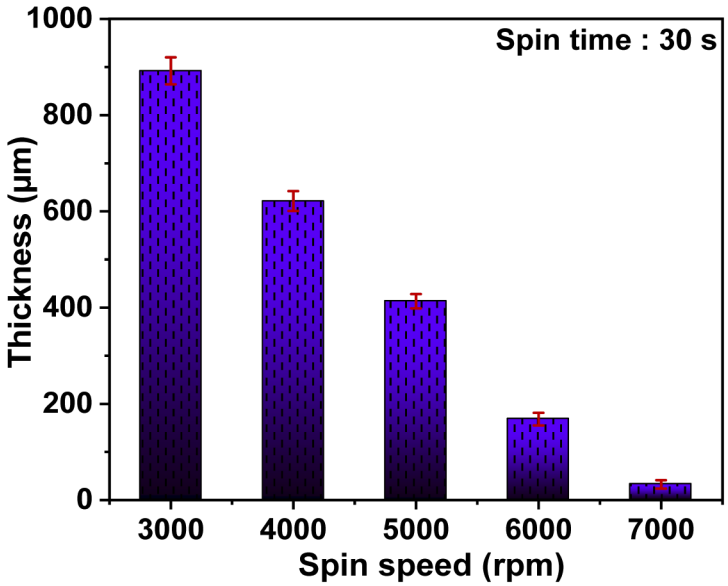

Fig. 3. Variation in hydrogel thickness with change in rotational speed of spin coating machine for a fixed duration (30 s).

The cavity length of the interferometer has been calculated to be 146 μm (λ_1=1523.12 nm and λ_2 = 1531.07 nm, exhibited in Fig. 4(a)), which is nearly the same as that obtained from microscopic measurement, as shown in Fig. 4(g). In addition, the optimized thickness of hydrogel is 642.03 μm shown in Fig. 4(f). Figures 4(a) and 4(b) show the spectral response of three sensors and broadband source, respectively. Three sensors were fabricated with different hydrogel thicknesses, such as 357.24 μm, 642.03 μm, and 921.89 μm. The inner surfaces of the hydrogel corresponding to three probes have been depicted in Figs. 4(b), 4(c), and 4(d). These different thicknesses were obtained based on different spinning speeds for fixed time duration of 30 s during spin coating. However, the interference pattern corresponding to the probe with gel thickness of 642.03 μm has better visibility and stability than other probes. The surface of the hydrogel is not smooth enough for thicknesses 922 μm and 357 μm. This is due to the fact that these cavities have been obtained for speed rather than the optimized rotational speed of the spin coating machine.

3.3. Experimental setup

The experimental set up for pH sensing is shown in Fig. 2(d). The system consists of a BBS (home-made, with the maximum output power of 3 mW), a circulator (6015-3-APC, Thorlabs Inc, New Jersey, USA), and an OSA (AQ6370D, YOKOGAWA, Tokyo, Japan) with a spectral resolution of 0.05 nm. Light is launched into the sensor head through one port of the circulator, and the reflected light from the tip of the probe is coupled to OSA through another port of the circulator.

Optics EXPRESS

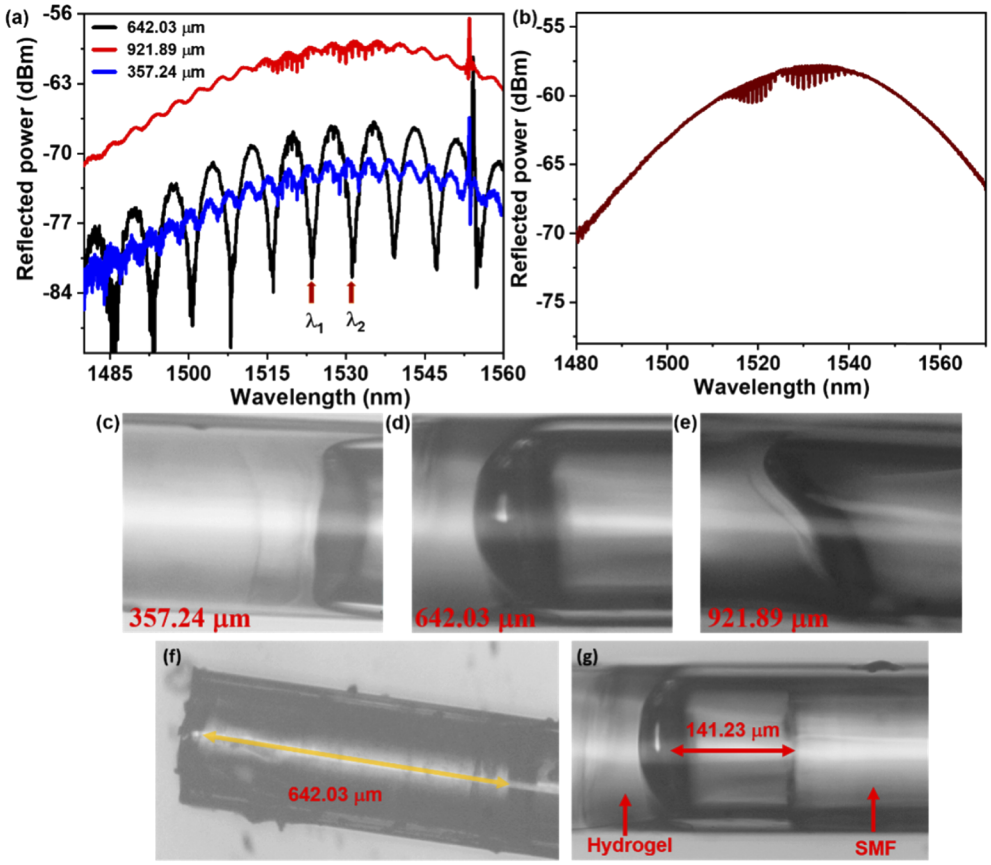

Fig. 4. (a) Reflected spectrum pattern of the probe with hydrogel thickness of 357.24 μm, 642.03 μm, and 921.89 μm respectively. (b) interference pattern of BBS. (c), (d) and (e) show the inner surface probes having hydrogel thickness of 357.24 μm, 642.03 μm, and 921.89 μm respectively. (f) and (g) are the optical microscope view of the optimized sensor showing thickness of hydrogel and cavity length respectively.

4. Results and discussion

Figure 5(a) shows the spectral response of the probe upon immersion into solutions with different pH values. Solutions with pH values varying from 1 to 7 were considered for the experiment. When the pH of the solution is decreased from 7 to 1, the interference minima shows blue shift. The blue shift can be attributed to hydrogel swelling for solutions with lower pH values, and this expansion leads to a decrease in cavity length. The above process was repeated for three cycles, and the average sensitivity was found to be 0.30 nm/pH shown in Fig. 5(b), which is higher than previously reported results [25].

Further, the sensor response time (see Fig. 6) is analyzed by dipping it into the liquid with pH 7 followed by liquid with pH 5. The response time of the sensor was found to be 20 s (T_f, falling time) for a change in pH of the solution from 7 to 5 and the recovery time (change in PH from 5 to 7) was around 15 s (T_r, rising time). The sharp peak in the graph refers to the duration for which sensor is in the air (during the change in solution). The sensor's quick response can be attributed to the direct interaction between the hydrogen ions and hydrogel, which led to the hydrogel swelling. In contrast, other methods based on FBG [6] and surface plasmon resonance [8] have longer response time because the response in these sensors is based on fiber hydrogel

Optics EXPRESS

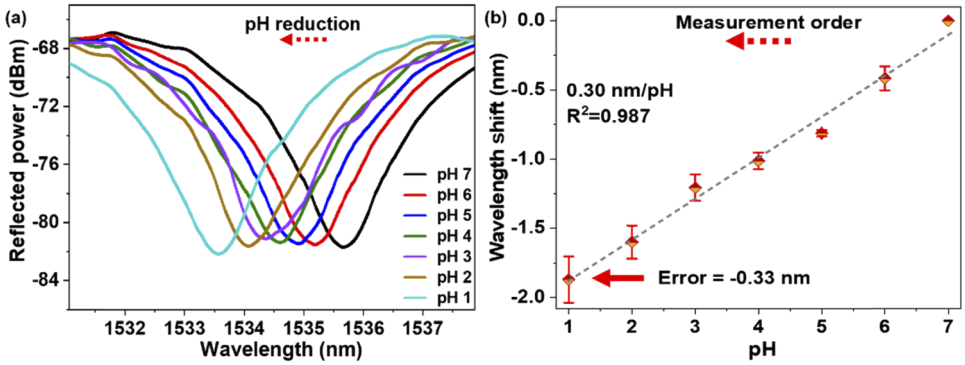

Fig. 5. (a) Spectral response of the sensor for pH varying from 1 to 7, (b) Sensitivity performance of the sensor for variation in pH from 7 to 1.

compression. The comparison of the performance of our probe with other reported probes in the acidic range is summarized in Table 1.

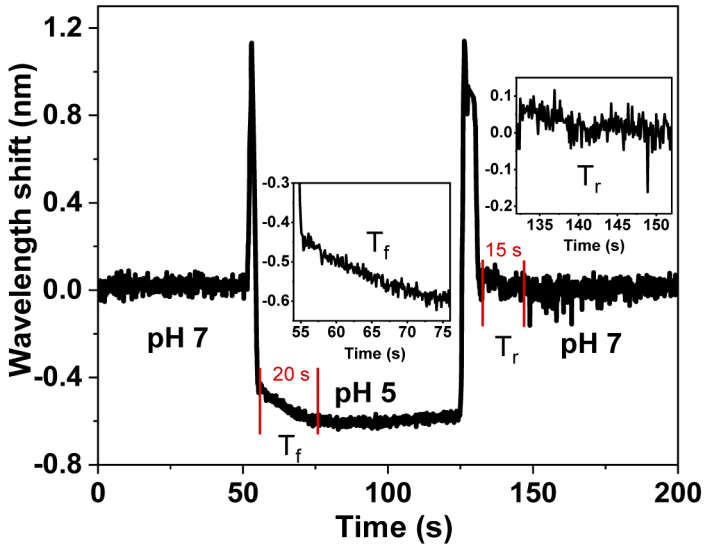

Fig. 6. Response time of the proposed sensor for change in pH from 5 to 7.

The sensor temperature sensitivity performance is shown in Fig. 7. In order to carry out the probe response to change in environmental temperature, the probe is placed in a furnace where the temperature was varied from 25°C to 40°C. It is to be noted here that the FBG embedded in SMF could be used to calibrate temperature response due to its insensitiveness towards pH measurement. The length of the integrated FBG was 5 mm and was written at a distance of 7 mm from the SMF tip. The shift of interference pattern (inset) along with variation in shift with temperature for the FP cavity has been shown in Fig. 7(a). In contrast, the shift in FBG peak (inset) and variation in shift with temperature change have been displayed in Fig. 7(b). The FP cavity temperature sensitivity has been found to be -0.56 nm/°C while that of FBG peak has been found to be 9 pm/ °C. Considering both these parameters, the cross temperature sensitivity found to be ~-1.87 pH/°C.

Optics EXPRESS

Table 1. Performance of the sensor compared to the existed fiber optic sensor in the acidic range.

Method	Coated material	Fabrication complexity	pH range	Sensitivity	Response time	References
FBG based POF	PEGDA	Medium	2-6.5	−0.34 nm/pH	$T_r = 30$ s	[6]
FBG based on SMF	Hydrogel	Medium	4-7	73 ± 2 pm/pH	$T_f = 2.5$ min $T_r = 4.5$ min	[25]
SPR based pH sensor	PAH/PAA	Complex	3-7	0.453 a.u/pH	-	[27]
FPIbuilt pH sensor using PCF and SMF	PVA/PAA	Complex	4.1-6.9	11 nm/pH	-	[14]
FP cavity based on SMF and capillary	Hydrogel	Simple	1-7	0.30 nm/pH	$T_f = 20$ s $T_r = 15$ s	This study

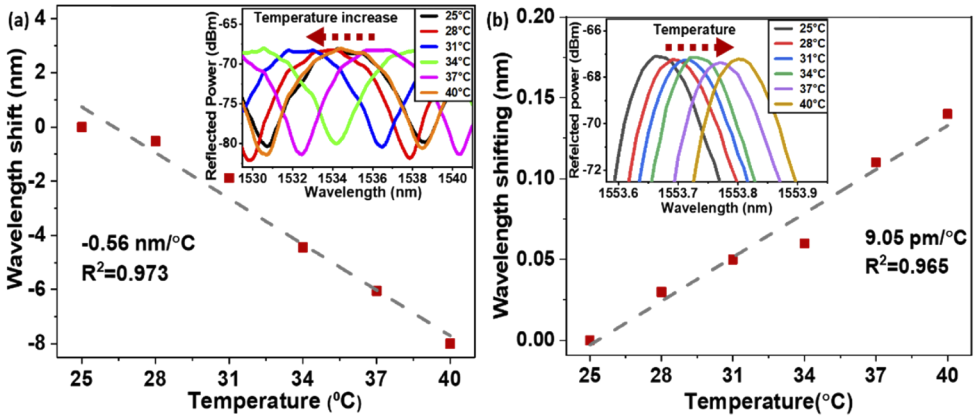

Fig. 7. Temperature response of FP cavity (a), and embedded FBG (b). The inset of Fig (a) and (b) show the shift in the FP interference spectrum and FBG peak, respectively.

5. Conclusion

In summary, this work has offered a simple, compact, and quick responsive optical fiber pH sensor based on the FP cavity. The sensor fabrication involves the coating of UV cured pH-sensitive hydrogel at the tip of the capillary and insertion of FBG embedded SMF into the capillary. The hydrogel length was characterized by the spin coating method, where the optimized thickness was found at spin speed of 4000 rpm. A blue shift in the interference spectrum was detected as the sensor submerged into the aqueous solution with different pH values. The sensor sensitivity was found to be 0.30 nm/pH, and the response is linear. The response time has been found to be 20 s (falling time) and 15 s (rising time) for a change in pH value from 7 to 5 and 5 to 7, respectively. The temperature response of the sensor has been analyzed by tracking the shift of interference pattern corresponding to FP cavity and the wavelength shift of FBG peak. The FP cavity temperature sensitivity and the FBG have been found to be -0.56 nm/°C and 9 pm/°C, respectively. The cross temperature sensitivity can be calculated by tacking the FBG peak during the experimental measurement of pH. Therefore, these results are promising to build a reliable FP cavity-based fiber optic pH sensor in the acidic range. However, the performance of the sensor could be further improved using novel pH sensitive material.

Funding

Research Grants Council, University Grants Committee (15211317).

Optics EXPRESS

Disclosures

The authors declare that there are no conflicts of interest related to this article.

References

1. M. Islam, M. M. Ali, M.-H. Lai, K.-S. Lim, and H. Ahmad, "Chronology of Fabry-Perot interferometer fiber-optic sensors and their applications: a review," Sensors **14**(4), 7451–7488 (2014).
2. B. Gu, M. Yin, A. P. Zhang, J. Qian, and S. He, "Biocompatible fiber-optic pH sensor based on optical fiber modal interferometer self-assembled with sodium alginate/polyethylenimine coating," IEEE Sens. J. **12**(5), 1477–1482 (2012).
3. O. S. Wolfbeis, "Fiber-optic chemical sensors and biosensors," Anal. Chem. **80**(12), 4269–4283 (2008).
4. S. A. Grant and R. S. Glass, "A sol–gel based fiber optic sensor for local blood pH measurements," Sens. Actuators, B **45**(1), 35–42 (1997).
5. X. Yang and L. Wang, "Fluorescence pH probe based on microstructured polymer optical fiber," Opt. Express **15**(25), 16478–16483 (2007).
6. X. Cheng, J. Bonefacino, B. Guan, and H. Tam, "All-polymer fiber-optic pH sensor," Opt. Express **26**(11), 14610–14616 (2018).
7. M. Engholm, K. Hammarling, H. Andersson, M. Sandberg, and H.-E. Nilsson, "A bio-compatible fiber optic pH sensor based on a thin core interferometric technique," in *Photonics*, (Multidisciplinary Digital Publishing Institute, 2019), 11.
8. S. K. Mishra and B. D. Gupta, "Surface plasmon resonance based fiber optic pH sensor utilizing Ag/ITO/Al/hydrogel layers," Analyst **138**(9), 2640–2646 (2013).
9. X. Cheng, J. N. Dash, D. S. Gunawardena, L. Htein, and H.-Y. Tam, "Silicone Rubber Based Highly Sensitive Fiber-Optic Fabry–Perot Interferometric Gas Pressure Sensor," Sensors **20**(17), 4927 (2020).
10. J. L. Elster, M. E. Jones, M. K. Evans, S. M. Lenahan, C. A. Boyce, W. H. Velander, and R. VanTassell, "Optical fiber extrinsic Fabry-Perot interferometric (EFPI)-based biosensors," in *Biomedical Diagnostic, Guidance, and Surgical-Assist Systems II*, (International Society for Optics and Photonics, 2000), 105–112.
11. M. Wang, M. Yang, J. Cheng, G. Zhang, C. Liao, and D. Wang, "Fabry–Perot interferometer sensor fabricated by femtosecond laser for hydrogen sensing," IEEE Photonics Technol. Lett. **25**(8), 713–716 (2013).
12. G. Zhang, M. Yang, and M. Wang, "Large temperature sensitivity of fiber-optic extrinsic Fabry–Perot interferometer based on polymer-filled glass capillary," Opt. Fiber Technol. **19**(6), 618–622 (2013).
13. L. Zhao, Y. Zhang, Y. Chen, and J. Wang, "Composite cavity fiber tip Fabry-Perot interferometer for high temperature sensing," Opt. Fiber Technol. **50**, 31–35 (2019).
14. Y. Zheng, X. Dong, K. Ni, C. C. Chan, and P. P. Shum, "Miniature pH sensor based on optical fiber Fabry-Perot interferometer," in *The 7th IEEE/International Conference on Advanced Infocomm Technology*, (IEEE, 2014), 192–197.
15. J. Goicoechea, C. Zamarreño, I. Matias, and F. Arregui, "Utilization of white light interferometry in pH sensing applications by mean of the fabrication of nanostructured cavities," Sens. Actuators, B **138**(2), 613–618 (2009).
16. A. Patel and K. Mequanint, "Hydrogel biomaterials," in *Biomedical engineering-frontiers and challenges* (IntechOpen, 2011).
17. A. Richter, G. Paschew, S. Klatt, J. Lienig, K.-F. Arndt, and H.-J. P. Adler, "Review on hydrogel-based pH sensors and microsensors," Sensors **8**(1), 561–581 (2008).
18. J. Ricka and T. Tanaka, "Swelling of ionic gels: quantitative performance of the Donnan theory," Macromolecules **17**(12), 2916–2921 (1984).
19. R. A. Siegel and B. A. Firestone, "pH-dependent equilibrium swelling properties of hydrophobic polyelectrolyte copolymer gels," Macromolecules **21**(11), 3254–3259 (1988).
20. J. Ma, J. Ju, L. Jin, W. Jin, and D. Wang, "Fiber-tip micro-cavity for temperature and transverse load sensing," Opt. Express **19**(13), 12418–12426 (2011).
21. T. Wei, Y. Han, Y. Li, H.-L. Tsai, and H. Xiao, "Temperature-insensitive miniaturized fiber inline Fabry-Perot interferometer for highly sensitive refractive index measurement," Opt. Express **16**(8), 5764–5769 (2008).
22. T. Wei, Y. Han, H.-L. Tsai, and H. Xiao, "Miniaturized fiber inline Fabry-Perot interferometer fabricated with a femtosecond laser," Opt. Lett. **33**(6), 536–538 (2008).
23. B. Wang, J. Tian, L. Hu, and Y. Yao, "High sensitivity humidity fiber-optic sensor based on all-agar Fabry–Perot interferometer," IEEE Sens. J. **18**(12), 4879–4885 (2018).
24. J. N. Dash and R. Jha, "Fabry–Perot cavity on demand for hysteresis free interferometric sensors," J. Lightwave Technol. **34**(13), 3188–3193 (2016).
25. J. Janting, J. K. Pedersen, G. Woyessa, K. Nielsen, and O. Bang, "Small and robust all-polymer fiber Bragg grating based pH sensor," J. Lightwave Technol. **37**(18), 4480–4486 (2019).
26. A. Scheludko, B. Toshev, and D. Bojadjiev, "Attachment of particles to a liquid surface (capillary theory of flotation)," J. Chem. Soc., Faraday Trans. 1 **72**(0), 2815–2828 (1976).
27. K. M. Yatim, G. Krishnan, H. Bakhtiar, S. Daud, and S. W. Harun, "The pH sensor based optical fiber coated with PAH/PAA," in *Journal of Physics: Conference Series*, (IOP Publishing, 2019), 012021.